energy and band gap due to repulsion between atoms on A sites and atoms on B sites after atoms on B site having displacements are not considered.

perovskites. According to the effects on the band gap within the considered range of distorted amplitudes, these single modes in cubic $ATiO_3$ can be roughly grouped into three types: (i) Jahn-Teller, off-center displacements result in gradually band gap blueshift as the amplitude of distortion increase, (ii) whereas the breathing mode lead to gradually band gap redshift as amplitude distortion increase, (iii) the lattice expansion and octahedral rotation mode can either result in band gap blueshift or redshift, which depends on the range of distorted amplitudes. Specifically, for cubic $ATiO_3$ (A=Ca, Sr, Ba), compression of lattice constants can result in band gap blueshift, lattice expansion can result in band gap redshift; octahedral tilting angle in range of 0-8° can result in band gap blueshift, while the redshift occurs when rotation angle over 8°. For halide perovskites $CsBI_3$ (B=Pb, Sn), these single modes can also be classified into three types: (i) octahedral rotation, B site off-center can result in band gap blueshift as amplitudes of distortion increase; (ii) Jahn-Teller distortion and breathing modes can lead to band gap redshift as amplitude increase; (iii) the compression of lattice constant lead to band gap decrease and lattice expansion result in band gap blueshift. The trends of energy lowering and band gap changes because of single-mode changes are not unique for perovskites, depending on the specific compositions of ABX_3 perovskites.

Figure S-1. Single-mode (one at the time) examination of potential energy lowering symmetry breaking in cubic oxide perovskites BaTiO$_3$ (a, c), SrTiO$_3$ (b, d, g) and CaTiO$_3$ (e, f, h) due to Distortions Off Wyckoff Positions (DOWPs) by DFT at T=0 using the PBEsol functional. Enthalpy changes as functions of the amplitude of (a, b, e) octahedral breathing mode; (c, d, f) lattice expansion; and (g, h) Jahn-Teller distortion (Q2+, Q2- modes). For lattice expansions on a, ab, abc directions, we use the minimal unit cells containing 1 fu/cell that already accommodate such a distortion, whereas evaluation of symmetry breaking Jahn-Teller distortions, breathing modes leading to disproportionation of octahedra, as well as the anti-ferroelectric displacement are all symmetry disallowed in the minimal unit cell structure, and are illustrated here for the 8 fu/cell. Such calculations involve a constrained energy minimization, where the shape and lattice vectors of the cell are kept as that of the global phase being investigated (here, cubic). All modes depicted of single modes are not energy lowering mode.

Figure S-2. Single-mode (one at the time) examination of possible energy lowering symmetry breaking in cubic halide perovskites CsSnI₃ (a, b, c, d, h) and CsPbI₃ (e, f, g) due to Distortions Off Wyckoff Positions (DOWPs) by DFT at T=0 using the PBEsol functional. Enthalpy changes as functions of the amplitude of (a) B site off-center displacements; (b) octahedral rotation; (c, e) octahedral breathing mode; (f, h) lattice expansion; and (d, g) Jahn-Teller distortion (Q2+, Q2- modes). All the single modes depicted here except tilting modes in CsSnI₃ cannot result in internal energy lowering.

Figure S-3. Cubic oxide perovskites: Band gap changes as a function of different modes (a, b) breathing mode and (c, d) lattice expansion for cubic $BaTiO_3$ and cubic $CaTiO_3$.
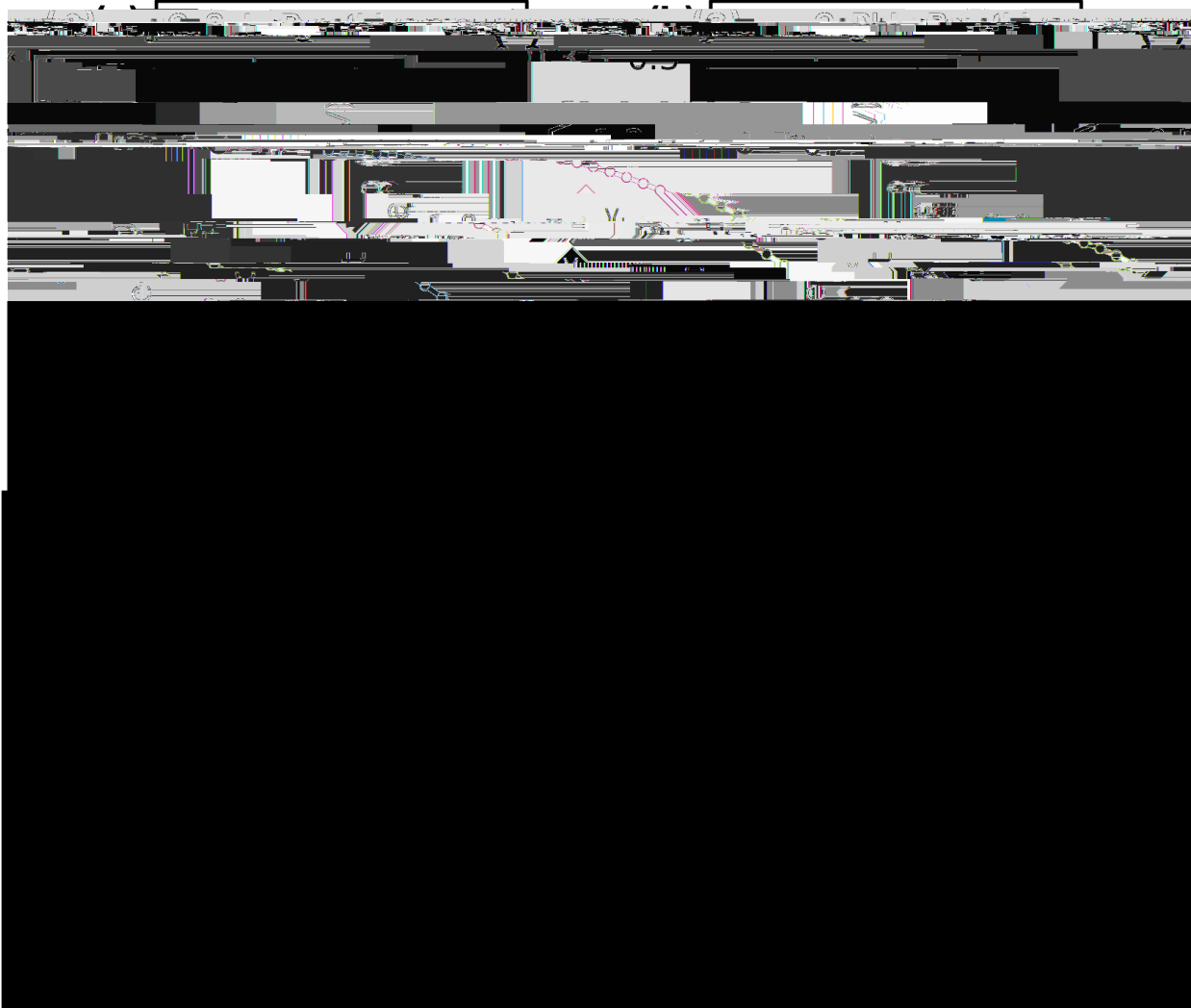
Figure S-4. Cubic halide perovskites: Band gap changes as a function of different modes (a, b) breathing mode and (c, d) lattice expansion for cubic CsPbI₃ and cubic CsSnI₃.
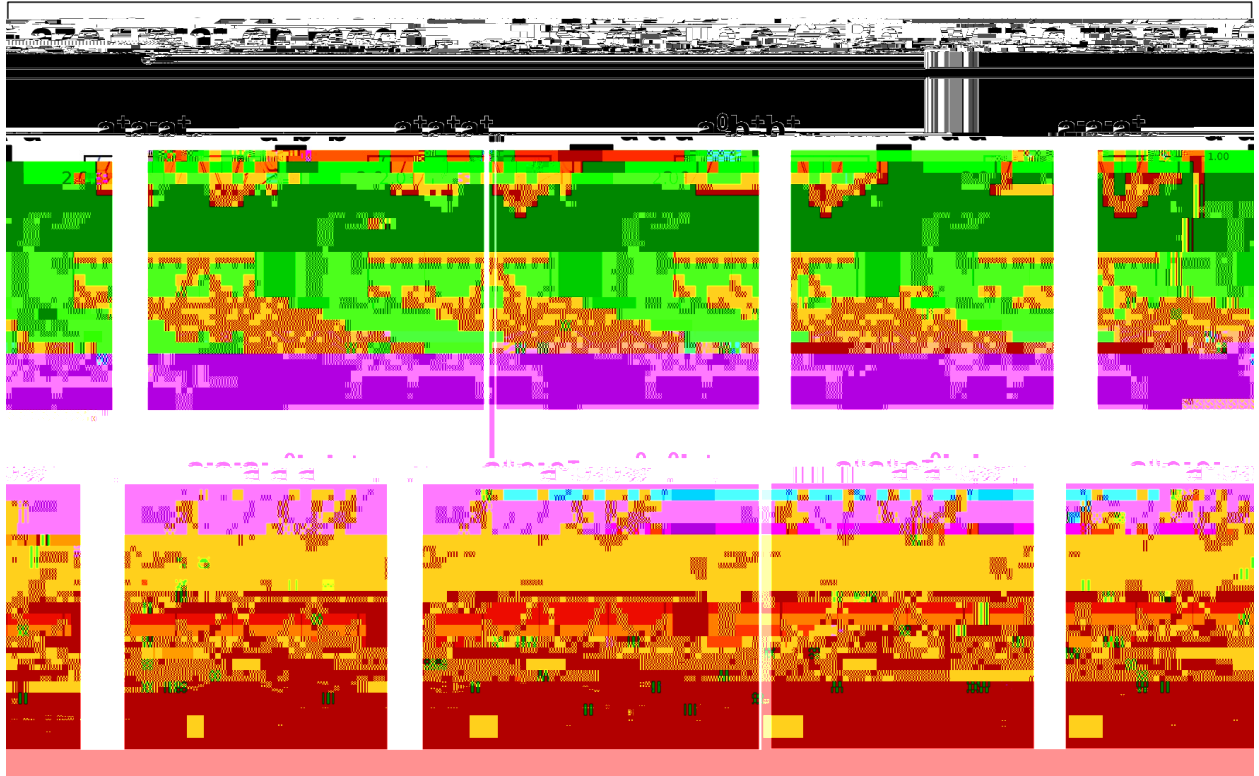
Figure S-5. The effect band structure (EBS) of $CsPbI_3$ in 2×2×2 supercell with single Glazer notation. For cubic $CsPbI_3$, the EBS always shows a direct gap at the R point. Different octahedral rotation modes result in similar band edges states, which is significantly different from $CaTiO_3$ (Fig. 9 main text)

References:

[1] G. Kresse, J. Furthmüller, Phys. Rev. B 54 (1996) 11169–11186.

[2] X.-G. Zhao, K. zhou, B. Xing, R. Zhao, S. Luo, T. Li, Y. Sun, G. Na, J. Xie, X. yang, X. Wang, X. Wang, X. He, J. Lv, Y. Fu, L. Zhang, ArXiv:2103.07957 (2021).

[3] J.P. Perdew, A. Ruzsinszky, G.I. Csonka, O.A. Vydrov, G.E. Scuseria, L.A. Constantin, X. Zhou, K. Burke, Phys. Rev. Lett. 100 (2008) 136406.

[4] A.M. Glazer, Acta Cryst B, Acta Cryst Sect B, Acta Crystallogr B, Acta Crystallogr Sect B, Acta Crystallogr B Struct Crystallogr Cryst Chem, Acta Crystallogr Sect B Struct Crystallogr Cryst Chem 28 (1972) 3384–3392.

[5] J. Varignon, M. Bibes, A. Zunger, Nature Communications 10 (2019) 1658.

[6] D. Frenkel, B. Smit, Understanding Molecular Simulation: From Algorithms to Applications, Elsevier, 2001.

[7] C.L. Farrow, P. Juhas, J.W. Liu, D. Bryndin, E.S. Božin, J. Bloch, T. Proffen, S.J.L. Billinge, J. Phys.: Condens. Matter 19 (2007) 335219.

[8] A.N. Beecher, O.E. Semonin, J.M. Skelton, J.M. Frost, M.W. Terban, H. Zhai, A. Alatas, J.S. Owen, A. Walsh, S.J.L. Billinge, ACS Energy Lett. 1 (2016) 880–887.

[9] G.E. Eperon, G.M. Paternò, R.J. Sutton, A. Zampetti, A.A. Haghighirad, F. Cacialli, H.J. Snaith, J. Mater. Chem. A 3 (2015) 19688–19695.

[10] I. Chung, J.-H. Song, J. Im, J. Androulakis, C.D. Malliakas, H. Li, A.J. Freeman, J.T. Kenney, M.G. Kanatzidis, J. Am. Chem. Soc. 134 (2012) 8579–8587.

[11] V.V. Lemanov, A.V. Sotnikov, E.P. Smirnova, M. Weihnacht, R. Kunze, Solid State Communications 110 (1999) 611–614.

[12] M. Yashima, M. Tanaka, J Appl Cryst 37 (2004) 786–790.

[13] K. Suzuki, K. Kijima, Journal of Alloys and Compounds 419 (2006) 234–242.

[14] F.W. Lytle, Journal of Applied Physics 35 (1964) 2212–2215.